J. Fluid Mech. (1996), vol. 328, pp. 67–93

Concentration waves and the instability of bubbly flows

By J. H. LAMMERS† AND A. BIESHEUVEL

J. M. Burgers Centre for Fluid Mechanics, University of Twente, P.O.Box 217, 7500 AE Enschede, The Netherlands

(Received 2 September 1994 and in revised form 2 July 1996)

This paper examines whether G. K. Batchelor's (1988) theory of the propagation of planar concentration disturbances and the occurrence of instabilities in uniform fluidized beds can be applied to bubbly flows. According to this theory the propagation of long weakly nonlinear gas volume concentration waves is governed by the Burgers equation. Experiments on the propagation of weak concentration shock waves and small, but finite, amplitude periodic waves are presented; good agreement is found with classic solutions of Burgers' equation. For example, the phenomenon of amplitude saturation, familiar from nonlinear acoustics, is established here for concentration waves. Batchelor's instability conditions are given for bubbly flows, and his model for the bulk modulus of elasticity of the dispersed phase is used to obtain estimates of the critical volume concentration at which a uniform bubbly flow becomes unstable to planar disturbances. Observations of the onset of instabilities of bubbly flow in a pipe are described, and compared with what would be expected from Batchelor's theory.

1. Introduction

Observations of bubbly flows in a vertical cylindrical pipe show that upon increasing the gas flow rate into the lower end of the pipe a uniform bubbly flow changes structure and becomes a kind of agitated, 'turbulent' bubbly flow. This turbulent flow is characterized by large collections of bubbles that violently move about in a kind of zig-zag motion. The transition first appears in the upper section of the pipe, and upon further increasing the gas flux the point of transition moves downwards. Since a larger gas flux leads to a larger gas volume concentration everywhere in the pipe, and since the volume concentration increases with height along the tube, due to the loss of hydrostatic head, this suggests that there is a critical value of the gas volume concentration associated with the flow transition. For still higher gas fluxes the gas bubbles within the region of turbulent flow begin to coalesce, and eventually large gas plugs are formed that fill the entire cross-section of the pipe. The flow changes into a regime in which gas plugs move upwards with high speed, separated by regions with an approximately uniform bubbly fluid.

The above-described behaviour may be compared to what is observed in liquid-fluidized beds. Didwania & Homsy (1981) conclude from experiments in a narrow, two-dimensional bed that increasing the liquid flow rate changes the regime of

† Present address: Philips Research Laboratories, Prof. Holstlaan 4, 5656 AA Eindhoven, The Netherlands.

uniform fluidization into a wavy regime. The voidage waves first appear in the upper part of the bed; at higher liquid flow rates the waves are also observable near the distributor. Initially the waves have planar form, but as they travel upwards they develop transverse structure. At higher liquid flow rates the bed becomes 'turbulent', and occasionally 'bubbles', regions devoid of particles, appear. Finally, a sudden transition to the bubbly regime of fluidization takes place. In wider beds the transition is slightly different (El-Kaissy & Homsy 1976). In that case the planar voidage waves in the lower part of the bed become convex as they travel upwards, start to zig-zag, and coalesce with other waves. Then another coherent wave forms, which eventually breaks up into small high-voidage regions or into bubble-like clusters.

So it seems that the transition towards a 'turbulent' bubbly flow regime and the formation of regions with large numbers of bubbles resembles what is described by Didwania & Homsy (1981), but for the difference, of course, that in fluidized beds the particles are expelled from, rather than attracted to, certain regions within the turbulent flow. Note that no developing plane wave trains in the bubbly flow have been observed by us; occasionally regions of high bubble volume concentration could be seen, that executed zig-zag motions as they moved upwards with high velocity into the 'turbulent' part of the flow, and these perhaps resemble the structures decribed by El-Kaissy & Homsy (1976). It is generally agreed that the initial stage of the transition from uniform fluidization to a bubbly type of fluidization is due to an instability of the flow to planar voidage disturbances, and it is reasonable to examine whether this is also the case in the flow transition of bubbly flows.

Now, in a beautiful analysis of the conditions under which uniform fluidized beds are unstable to planar voidage disturbances Batchelor (1988) showed that when spatial gradients are sufficiently small, the mass and momentum conservation equations of the particles, in a reference frame in which there is no net volume flux of material, are given by

$$\frac{\partial \phi}{\partial t} + V\frac{\partial \phi}{\partial x} + \phi\frac{\partial V}{\partial x} = 0, \tag{1.1}$$

$$\phi(1+\theta)\left(\frac{\partial V}{\partial t} + V\frac{\partial V}{\partial x}\right) - \phi\zeta V\frac{\partial V}{\partial x} + Q\frac{\partial \phi}{\partial x} - \frac{\partial}{\partial x}\left(\phi\eta\frac{\partial V}{\partial x}\right) = -\frac{\gamma\tilde{g}}{U}\phi(V-U). \tag{1.2}$$

Here ϕ and V denote the volume concentration and the mean velocity of the particles, $U(\phi)$ is the mean velocity of the particles in a homogeneous dispersion with volume concentration ϕ when the particles move only under the action of gravity. The constant γ depends on the functional relationship between the mean frictional force and the mean particle velocity under uniform conditions. It takes a value between 1 and 2, with the value 1 when the flow around the particles is described by the Stokes equations, and the value 2 in the case of large particle Reynolds numbers. The position-coordinate is positive in the *downward* direction, and the reduced gravity is defined by

$$\tilde{g} = g\frac{\rho_p - \rho_f}{\rho_p},$$

in which ρ_p and ρ_f respectively denote the density of the particles and the fluid (gas or liquid).

The first two terms on the left-hand side of (1.2) represent the acceleration reaction of the particles in a uniform suspension. The functions $\theta(\phi)$ and $\zeta(\phi)$ are related to the added mass coefficient $C(\phi)$ through

$$\theta(\phi) = \frac{\rho_f}{\rho_p} C(\phi), \quad \text{and} \quad \zeta(\phi) = \frac{\rho_f}{\rho_p} \phi \left(\frac{\mathrm{d}C}{\mathrm{d}\phi} \right).$$

The other two terms in the momentum conservation equation represent the mean force per unit mass of the particles which arises in a non-uniform dispersion because of momentum transport by velocity fluctuations of the particles, and by forces which the particles exert on each other hydrodynamically; $\phi\rho_p Q(\phi)$ is the bulk modulus of elasticity of the particles and $\phi\rho_p\eta(\phi)$ is an effective particle viscosity. These express in the usual manner the resistance to deformation of the particle configuration, i.e. of their relative positions and velocities.

The arguments used by Batchelor to formulate these conservation equations apply equally well to bubbly flows. Then one would prefer the position-coordinate to be positive *upwards*, which is achieved simply by redefining the reduced gravity as

$$\tilde{g} = g \frac{\rho_l - \rho_g}{\rho_g},$$

where now ρ_p has been replaced by ρ_g, the density of the gas bubbles, and ρ_f by ρ_l, the liquid density.

In this paper we try to verify Batchelor's theory by studying the propagation of concentration waves in uniform (stable) bubbly flows, and by examining the onset of transition. In §2 it is shown that the propagation of weakly nonlinear long-wavelength disturbances in uniform bubbly flows is governed by the Burgers equation. In §3 Batchelor's stability criteria are given, followed by a brief derivation of the equations describing the development of planar weakly nonlinear unstable disturbances. At present it does not seem to be possible to make quantitative predictions of the critical value of the volume concentration at which the instability occurs for the bubbly flows that we have studied experimentally. But some insight is gained from estimates for bubbly flows with small, approximately spherical bubbles; these are given in §4. That the Burgers equation applies is demonstrated in experiments on step-like and periodic concentration disturbances, for which well-known solutions of the Burgers equation are available from the theory of nonlinear acoustics. The measurement techniques and the methods of data analysis are described in §5 and §6, followed by a description of the experimental results on concentration wave propagation in §7, and the transition to turbulent bubbly flow in §8. We conclude with a summary.

2. Concentration waves

Suppose that a uniform bubbly fluid is characterized by a gas volume concentration ϕ_0 and a mean bubble velocity $U(\phi_0) \equiv U_0$, the latter defined with respect to a zero-volume-flux reference frame. To obtain a description of the disturbed flow we use the velocity U_0 and either the time scale T or the length scale $\lambda \simeq U_0 T$ of the imposed disturbances to render the conservation equations (1.1) and (1.2) dimensionless. These become

$$\frac{\partial \phi}{\partial \bar{t}} + \bar{V} \frac{\partial \phi}{\partial \bar{x}} + \phi \frac{\partial \bar{V}}{\partial \bar{x}} = 0, \tag{2.1}$$

$$\phi(1+\theta)\left(\frac{\partial \bar{V}}{\partial \bar{t}}+\bar{V}\frac{\partial \bar{V}}{\partial \bar{x}}\right)-\phi\zeta\bar{V}\frac{\partial \bar{V}}{\partial \bar{x}}+\bar{Q}\frac{\partial \phi}{\partial \bar{x}}-\frac{1+\theta_0}{R}\frac{\partial}{\partial \bar{x}}\left(\frac{\phi\bar{\eta}}{\bar{\eta}_0}\frac{\partial \bar{V}}{\partial \bar{x}}\right)$$

$$=-\frac{1+\theta_0}{F}\phi\left(\frac{\bar{V}-\bar{U}}{\bar{U}}\right). \tag{2.2}$$

Here we have introduced the non-dimensional variables

$$\bar{t}=tU_0/\lambda, \quad \bar{x}=x/\lambda, \quad \bar{V}=V/U_0, \quad \bar{U}=U/U_0, \quad \bar{Q}=Q/U_0^2, \quad \bar{\eta}=\eta/U_0\lambda;$$

the suffix 0 means that the functions are to be evaluated at the volume fraction of the undisturbed flow, and the dimensionless numbers F and R are defined as

$$F=\frac{(1+\theta_0)U_0^2}{\gamma|\tilde{g}|\lambda}, \quad R=\frac{(1+\theta_0)|U_0|\lambda}{\eta_0}.$$

The first number can be interpreted as the ratio between the relaxation time of the bubbles, $(1+\theta)U/\gamma\tilde{g}$, and the time scale of the disturbances.

Batchelor proposes representing the particle viscosity η by

$$\eta=\beta a|U|, \tag{2.3}$$

with β a constant of order unity, and a denoting the radius of the particles. For bubbly flows a reasonable representation seems to be

$$\eta=\beta\frac{\rho_l}{\rho_g}a|U|.$$

The numbers F and R roughly scale as $\mathrm{F}\sim\xi(1+\theta)(a/\lambda)$, with particle Froude number $\xi=U_\infty{}^2/\gamma a|\tilde{g}|$, and $\mathrm{R}^{-1}\sim(1+\theta)^{-1}(a/\lambda)$ (for fluidized beds) or $\mathrm{R}^{-1}\sim a/\lambda$ (for bubbly flows), and thus should both be small for consistency with the use of a continuum approach and the application of Batchelor's theory.

If we assume then that $F\ll 1$ and $R\gg 1$, a first approximation is obtained by neglecting the left-hand side of (2.2). This yields $\bar{V}=\bar{U}$, and upon substitution in (2.1),

$$\frac{\partial \phi}{\partial x}+\frac{1}{c(\phi)}\frac{\partial \phi}{\partial t}=0, \qquad c(\phi)=U(\phi)+\phi\frac{\mathrm{d}U}{\mathrm{d}\phi}, \tag{2.4}$$

written again in physical variables. This represents a simple wave propagating with velocity $\phi(\mathrm{d}U/\mathrm{d}\phi)$ with respect to the bubbles. The solution can be obtained by Riemann's method, fitting in 'concentration shocks' where it becomes multi-valued with Whitham's rule (e.g. Whitham 1974). Since $\mathrm{d}c/\mathrm{d}\phi<0$ for bubbly flows, the shocks break backwards, i.e. the volume fraction in front of the shocks is larger than at the back. This description of the wave motion is that of the well-known Kynch (1952) theory of sedimentation waves.

An approximate equation describing weakly nonlinear waves can be derived by substituting

$$\phi=\phi_0+\epsilon\phi', \qquad \bar{V}=1+\epsilon\bar{V}'; \qquad \epsilon\ll 1, \tag{2.5}$$

in (2.1) and (1.2), and retaining only terms of $O(\epsilon)$ and $O(F)$. This yields, in physical variables,

$$\frac{\partial \phi'}{\partial x}+\left(\frac{1}{c_0}-\frac{c_1}{c_0^2}\phi'\right)\frac{\partial \phi'}{\partial t}=\frac{\mathscr{D}}{c_0^3}\frac{\partial^2\phi'}{\partial t^2} \tag{2.6}$$

with velocities c_0 and c_1 given by $c_0=c(\phi_0)$ and $c_1=\{\mathrm{d}c/\mathrm{d}\phi\}_{\phi=\phi_0}$. This is Burgers'

equation in the form appropriate to signalling problems. The diffusivity $\mathscr{D}$ is defined as

$$\mathscr{D} = \frac{U}{\gamma\tilde{g}}\left(Q - \phi^2\left\{\frac{\mathrm{d}U}{\mathrm{d}\phi}\right\}\left\{\frac{\mathrm{d}(1+\theta)U}{\mathrm{d}\phi}\right\}\right), \tag{2.7}$$

in which the functions of the volume concentration should be evaluated for $\phi = \phi_0$. (Note that this expression differs from that in Batchelor (1988, equation (3.18)), who does not include the acceleration-reaction effects.)

That Burgers' equation would be obtained could have been anticipated, of course, by recognizing that the assumption $R \gg 1$ puts the conservation equations in a form that is equivalent to the well-known wave-hierarchy problems studied by Lighthill and Whitham (see Whitham 1974). They showed that, in the order of approximation considered here, the 'dynamical' effects represented by the first three terms on the left-hand side of (2.2) have a diffusive effect on the 'kinematic' waves described by (2.4). Combination of weak nonlinearity in the simple wave description with linear diffusive effects yields Burgers' equation.

3. Instability

To obtain the conditions at which a uniform dispersion with volume concentration ϕ_0 is unstable to arbitrary infinitesimal perturbations one first linearizes the conservation equations. If it is next assumed that the disturbances are proportional to $\exp\{\mathrm{i}\kappa(x - ct)\}$, with complex phase speed c and real wavenumber κ, it follows that c has to satisfy the relation

$$(1+\theta)(c-U)^2 + (c-U)\left(\zeta U + \mathrm{i}\kappa\eta + \frac{\mathrm{i}\gamma\tilde{g}}{\kappa U}\right) - \left(Q + \frac{\gamma\tilde{g}}{\kappa U}\mathrm{i}W\right) = 0.$$

Here

$$W(\phi) = \phi\left(\frac{\mathrm{d}U}{\mathrm{d}\phi}\right),$$

and we have dropped the suffix 0. From the solution of this equation Batchelor (1988) then deduces that the condition for instability of the flow reads

$$\left\{\frac{\gamma\tilde{g}W}{\kappa^2\eta U + \gamma\tilde{g}} + \frac{\frac{1}{2}\zeta U}{1+\theta}\right\}^2 > \frac{Q}{1+\theta} + \frac{\frac{1}{4}\zeta^2U^2}{(1+\theta)^2}. \tag{3.1}$$

By considering the limit $\kappa \to \infty$, it becomes clear that a sufficient condition for instability is that $Q < 0$. This is as expected, because then the disperse phase has negative elasticity. To consider the case $Q > 0$, note that the left-hand side of the above expression obtains a maximum for some wavenumber $\kappa = \kappa_m$, which in general will depend on the values of the functions U, θ and η. Provided that

$$W + \frac{\frac{1}{2}\zeta U}{1+\theta} > 0, \tag{3.2}$$

a condition that holds for fluidized beds and also for bubbly fluids, this maximum is reached for $\kappa_m = 0$. Thus a dispersed flow will lose its stability at a value of the volume concentration ϕ such that

$$Q - W\{(1+\theta)W + \zeta U\} < 0.$$

Using the definitions of W and ζ this condition can be rewritten as

$$Q - \phi^2 \left\{ \frac{\mathrm{d}U}{\mathrm{d}\phi} \right\} \left\{ \frac{\mathrm{d}((1+\theta)U)}{\mathrm{d}\phi} \right\} < 0. \tag{3.3}$$

Comparing this with (2.7) it appears that the instability is associated with a negative effective diffusivity of long-wavelength disturbances. Strictly speaking equation (2.6) does not apply close to the critical value of the volume concentration, but as will be seen below the inference is still true.

For gas-fluidized beds $\rho_f \ll \rho_p$, so that $\theta \ll 1$. The condition for instability of the bed then reduces to

$$Q - \phi^2 \left\{ \frac{\mathrm{d}U}{\mathrm{d}\phi} \right\}^2 < 0.$$

Earlier models for the behaviour of gas-fluidized beds did not include a term expressing the bulk elasticity of the particles. The conclusion then must be that uniform gas-fluidized beds are always unstable. For bubbly fluids $\rho_l \gg \rho_g$, i.e. $\theta \gg 1$, and the condition for instability reads

$$Q - \frac{\rho_l}{\rho_g} \phi^2 \left\{ \frac{\mathrm{d}U}{\mathrm{d}\phi} \right\} \left\{ \frac{\mathrm{d}(CU)}{\mathrm{d}\phi} \right\} < 0.$$

Since in general the mean velocity of rise of the bubbles becomes less with increasing void fraction, it appears that when the bulk elasticity of the bubbles is absent in a description of the bubbly flow, the instability condition has the very simple form $\mathrm{d}(CU)/\mathrm{d}\phi < 0$. This expression can for instance be found in van Wijngaarden & Biesheuvel (1988). There is a simple interpretation. Suppose that an element of the dispersion is given a virtual displacement to a region with higher volume concentration. Since the impulse is conserved the change in the mean velocity of the bubbles in this element is

$$\delta v = -\frac{U}{C} \left\{ \frac{\mathrm{d}C}{\mathrm{d}\phi} \right\} \delta\phi.$$

On the other hand, the mean velocity of the surrounding bubbles, 'in equilibrium' because of a balance between gravity forces and viscous drag forces, is less than that of the bubbles at the original location by an amount

$$\delta U = \frac{\mathrm{d}U}{\mathrm{d}\phi} \delta\phi.$$

It follows that when $|\delta v| > |\delta U|$, i.e. when $\mathrm{d}(CU)/\mathrm{d}\phi < 0$, a virtual displacement to a region with higher concentration will cause the bubbles reach a velocity which is sufficient to push them to regions with still higher concentration; the system is unstable. Incidentally, note that when $\mathrm{d}(CU)/\mathrm{d}\phi > 0$ the flow can only be unstable when the bulk elasticity is negative.

Information on the correct expression for the bulk elasticity is absent, but Batchelor suggests by an elegant argument that it can be written as

$$\rho_p \phi Q(\phi) = \rho_p \phi \left(\frac{\gamma \tilde{g}}{U} D + \frac{\mathrm{d}(\phi H U^2)}{\mathrm{d}\phi} \right). \tag{3.4}$$

The first contribution arises from the hydrodynamic interaction forces between the particles which cause a diffusive flux of particles in the presence of a concentration gradient, with diffusivity $D(\phi)$. The second contribution represents transport of mean

particle momentum due to velocity fluctuations, with $H(\phi)$ a function that vanishes as $\phi \to 0$ and at closest packing. For bubbly flows the latter contribution is negligibly small of course, and one therefore expects that the condition $Q > 0$ is not violated.

It appears that what is required to obtain numerical estimates for the instability condition of uniform bubbly flows is a knowledge of the functions U, C, Q (or D). At present these estimates can only be given for flows with bubbles of approximately spherical shape; we will do so in the next section.

3.1. *Weakly nonlinear unstable waves*

A large number of papers have been written on the onset and the further evolution of instabilities in fluidized beds; with Batchelor's work as the most prominent exception these all used a two-fluid model as a starting point. Batchelor (1991, 1993) showed that as soon as *gas-fluidized beds* become linearly unstable to planar vertical disturbances the conditions are satisfied for a transverse structure to develop. On the other hand the experiments of Homsy and colleagues, described in the Introduction, clearly show that in *liquid-fluidized beds* the planar disturbances can grow to a considerable amplitude before they lose stability. It is therefore remarkable that almost all of the literature (e.g. Liu 1983; Ganser & Drew 1990; Harris & Crighton 1994) on the nonlinear development of planar unstable waves has been concerned with *gas-fluidized beds*; exceptions are Didwania & Homsy (1982) who look at liquid-fluidized beds, and Hayakawa, Komatsu & Tsuzuki (1994) who give an analysis for arbitrary values of the ratio ρ_f/ρ_p. It seems appropriate to briefly consider the equations governing the growth of the unstable waves as they follow from Batchelor's equations; a full discussion of their evolution is beyond the purpose of our paper.

First, it is useful to introduce the velocities

$$c_\pm = -\frac{\frac{1}{2}\zeta U}{1+\theta} \pm \left\{ \frac{Q}{1+\theta} + \frac{\frac{1}{4}\zeta^2 U^2}{(1+\theta)^2} \right\}^{1/2},$$

from which expression (2.7) for the diffusivity can be written as

$$\mathscr{D} = \frac{(1+\theta)U}{\gamma \tilde{g}}(c_+ - W)(W - c_-).$$

Batchelor's second criterion for instability (3.3), or equivalently $\mathscr{D} < 0$, therefore implies that instability occurs when the condition $(c_+ - W)(W - c_-) > 0$ is violated. Both for bubbly flows and fluidized beds condition (3.2) holds, which can also be written as $W - \frac{1}{2}(c_+ + c_-) > 0$. Clearly this implies that the instability is associated with c_- becoming less than W.

Next, to obtain estimates for the non-dimensional numbers F and R it is necessary to have an estimate of the characteristic length scale of the disturbances. From condition (3.1) it can be inferred that the wavenumber at neutral stability, $\kappa = \kappa_n$, is given by

$$\kappa_n{}^2 = \frac{\gamma \tilde{g}}{\eta U}\left(\frac{c_- - W}{|c_-|}\right).$$

The wavenumber at which the maximum growth rate occurs is roughly of this order. Thus if this would be an appropriate choice for the length scale we should have

$$\frac{\eta U}{\gamma \tilde{g} \lambda^2} = \frac{F}{R} = O\left(\frac{|c_- - W|}{|c_-|}\right). \tag{3.5}$$

By substituting (2.5) and using the scalings

$$F = O(\epsilon^{1/2}), \quad R^{-1} = O(\epsilon^{1/2}), \quad |(c_+ - W)(W - c_-)|/U^2 = O(\epsilon)$$

it is now straightforward to show that to first order the disturbances are described (in physical variables) by

$$\frac{\partial \phi'}{\partial t} + (U + W)\frac{\partial \phi'}{\partial x} = 0,$$

and to $O(\epsilon)$ by

$$\frac{\partial \phi'}{\partial t} + (U + W)\frac{\partial \phi'}{\partial x} + \left\{\frac{\mathrm{d}(U + W)}{\mathrm{d}\phi}\right\}\phi'\frac{\partial \phi'}{\partial x} + \frac{\eta U}{\gamma \tilde{g}} W \frac{\partial^3 \phi'}{\partial x^3} = 0, \tag{3.6}$$

where of course it is again understood that the coefficients are to be evaluated for the value of the volume concentration of the undisturbed flow. Initially the disturbances propagate with the 'kinematic wave speed' without change of form, but after a time of $O(\epsilon^{-1})$ nonlinear and dispersive effects become important. At this stage the waves are described by the Korteweg–de Vries equation.

To $O(\epsilon^{3/2})$ the pertinent equation becomes

$$\begin{aligned}\frac{\partial \phi'}{\partial t} + (U + W)\frac{\partial \phi'}{\partial x} + \left\{\frac{\mathrm{d}(U + W)}{\mathrm{d}\phi}\right\}\phi'\frac{\partial \phi'}{\partial x} + \frac{\eta U}{\gamma \tilde{g}} W \frac{\partial^3 \phi'}{\partial x^3} \\ = \mathscr{D}\frac{\partial^2 \phi'}{\partial x^2} + \left\{\frac{\mathrm{d}\mathscr{D}}{\mathrm{d}\phi}\right\}\frac{\partial}{\partial x}\left(\phi'\frac{\partial \phi'}{\partial x}\right) + \frac{\eta U}{\gamma \tilde{g}} W \frac{(1 + \theta)U}{\gamma \tilde{g}}\left(2W + \frac{\zeta}{1 + \theta}\right)\frac{\partial^4 \phi'}{\partial x^4}.\end{aligned} \tag{3.7}$$

This shows that the effects of a negative diffusivity become essential at a time of $O(\epsilon^{-3/2})$.

Similar evolution equations for instabilities in dispersions have recently been given by Hayakawa *et al.* (1994, see their equations (27) and (30)). These authors criticize the validity of other equations that have appeared in the literature on fluidized beds; our analysis seems to lend support to their criticism. The form of the evolution equations one obtains from an approximate analysis of the full equations depends on the choice of scaling of the dimensionless numbers F and R^{-1}, and on the value of the particle viscosity η in particular. Ganser & Drew (1990) and Harris & Crighton (1994) take the value of a number that plays a similar role as our number R, and which is also related to some kind of particle viscosity in their two-fluid model formulation, to be of order one. The formulation (2.3) of the particle viscosity as it is present in Batchelor's conservation equations, implies that R^{-1} must be small for consistency. Our experiments show beyond doubt that dispersive effects are negligibly small in the propagation of long-wavelength concentration waves; this would not have been the case if the value of R were of order one.

4. Estimates for dispersions with small bubbles

In the experiments that are described below we were not able to produce large numbers of bubbles with diameters less than 2.8 mm. For relatively large bubbles information on the functions that determine concentration wave propagation and the criteria for instability is lacking, so that a quantitative comparison between theory and experiments is not possible. However, estimates of the flow parameters of dispersions with small equally sized bubbles with equivalent radius in the range 0.5 mm to 1.3 mm rising in pure water can be given, and it is useful to do so.

The mean velocity of rise of the bubbles is usually expressed in the form

$$U(\phi) = U_\infty(1-\phi)^p, \tag{4.1}$$

where U_∞ is the velocity of a single bubble rising under the action of gravity in an infinite liquid, and p is a constant which depends on the physical properties of the two phases. For bubbly flows the value of p is usually found to be within the range 1.5–2.3. Single bubbles with equivalent radius less than 0.9 mm rise in a straight line and have oblate ellipsoidal shape. An approximate expression for their velocity has been derived by Moore (1965):

$$U_\infty = \frac{a^2 g}{9\nu G(\chi)}, \tag{4.2}$$

where χ is the ratio between the major axis and the minor axis, and

$$G(\chi) = \tfrac{1}{3}\chi^{4/3}(\chi^2-1)^{3/2}\frac{(\chi^2-1)^{1/2} - (2-\chi^2)\cos^{-1}\chi^{-1}}{(\chi^2\cos^{-1}\chi^{-1} - (\chi^2-1)^{1/2})^2}.$$

The deformation follows from (4.2) together with a relation for the Weber number

$$W(\chi) = \frac{2\rho_l U_\infty{}^2 a}{\sigma} = 4\frac{(\chi^3+\chi-2)(\chi^2\sec^{-1}\chi - (\chi^2-1)^{1/2})^2}{\chi^{4/3}(\chi^2-1)^3}, \tag{4.3}$$

where σ denotes the coefficient of surface tension. Bubbles with an equivalent radius in the range 0.9 mm to 1.4 mm perform a spiralling motion. The deformation can also be calculated to a good approximation from (4.2) and (4.3), where now expression (4.2) gives the (approximately constant) speed along the bubble trajectory; the mean speed of rise is about 10 % less (Duineveld 1994).

A good approximation for the function $C(\phi)$ is

$$C(\phi) = \tfrac{1}{2}\bar{Q}(\chi)\frac{1+(2/\bar{Q}(\chi))\phi}{1-\phi} \tag{4.4}$$

with

$$\bar{Q}(\chi) = 2\chi^2\frac{(\chi^2-1)^{1/2} - \cos^{-1}\chi^{-1}}{\chi^2\cos^{-1}\chi^{-1} - (\chi^2-1)^{1/2}}.$$

As already mentioned by far the most dominant contribution to the elasticity Q is the first term in expression (3.4). Not much is known about the function D; Batchelor proposes writing

$$D(\phi) = \alpha a|U| = \alpha a|U_\infty|(1-\phi)^p,$$

where α is a constant of order unity. With this choice the expression for the diffusivity of long-wavelength concentration waves

$$\mathscr{D} = D - \frac{U}{\gamma g}\phi^2\left\{\frac{\mathrm{d}U}{\mathrm{d}\phi}\right\}\left\{\frac{\mathrm{d}(CU)}{\mathrm{d}\phi}\right\}$$

becomes

$$\mathscr{D} = aU_\infty(1-\phi)^p\left\{\alpha - \xi p^2\phi^2(1-\phi)^{2(p-1)}\left(C - \frac{1-\phi}{p}\frac{\mathrm{d}C}{\mathrm{d}\phi}\right)\right\}$$

with ξ the bubble Froude number defined as

$$\xi = \frac{U_\infty{}^2}{\gamma a g}.$$

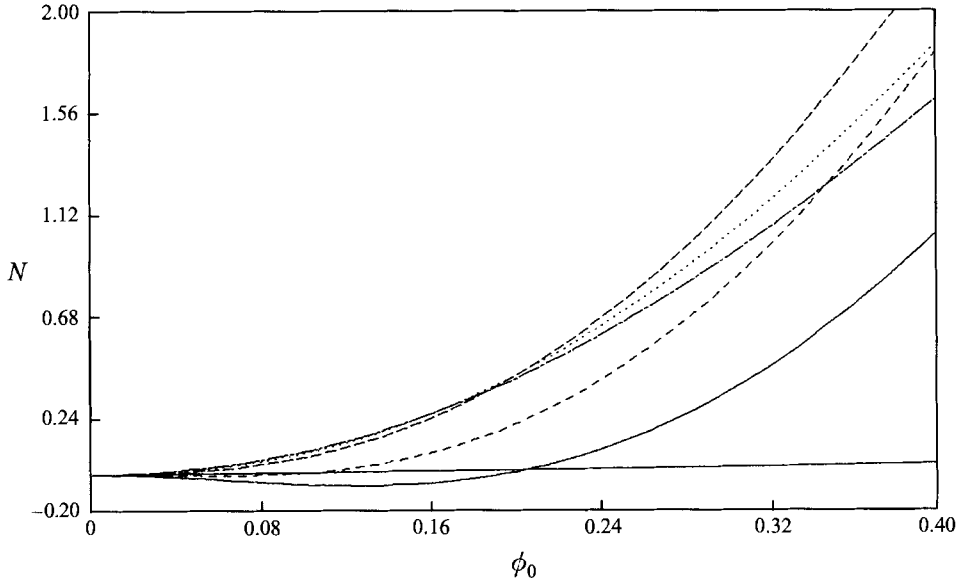

FIGURE 1. Stability criterion for dispersions of equally sized bubbles in water. The function $N(\phi)$ is evaluated for bubble radii 0.5 mm (solid curve), 0.7 mm (- -), 0.9 mm (– –), 1.1 mm (· · ·) and 1.3 mm (– · –). The critical volume concentration ϕ_c is determined by the point of intersection with a horizontal line $N = \alpha$; the flow is unstable for $\phi_0 > \phi_c$.

The condition for instability (3.3) reduces to

$$N(\phi) \equiv \xi p^2 \phi^2 (1-\phi)^{2(p-1)} \left(C - \frac{1-\phi}{p} \frac{\mathrm{d}C}{\mathrm{d}\phi} \right) > \alpha. \tag{4.5}$$

In figure 1 the function N is plotted for bubble radii between 0.5 mm and 1.3 mm, with the value of p equal to 2. If α is known one can draw a horizontal line $N = \alpha$ to find the critical value ϕ_c at which the flow first becomes unstable. The distance between this horizontal line and the curves is also a measure of the relative importance of bubble inertia and gradient diffusion to the attenuation of concentration waves; the latter appears to be the dominant effect for concentrations well below the critical. Note that ϕ_c strongly varies with the bubble size and the value of α, which will make it difficult to give accurate predictions of the critical volume concentration for practical systems. Also note once again, that in pipe flow experiments the volume concentration will increase along the pipe because the bubbles grow in size due to the loss of hydrostatic head; thus even though the flow may be stable in the lower part of the pipe, it may eventually become unstable higher up.

5. Experimental techniques

5.1. *Experimental facility*

The experimental facility in which Batchelor's (1988) theory was tested is basically the same set-up as was used by van Wijngaarden & Kapteyn (1990) for their experiments on concentration shock waves in dilute bubbly flows. It consists of a Perspex tube with 8 cm inner diameter and 5.5 m length, mounted on an inlet section in which bubbles are produced by injecting air through 150 needles with an inner diameter of 0.5 mm. Each of the needles (Hamilton) is placed in a small channel; by adjusting the water flow rate through these channels a bubbly fluid with nearly equally sized

bubbles is produced. The gas flow rate is set by three mass flow controllers (MKS) and the water flow rates, one past the needles and the other into the riser, are set by frequency-controlled (Scand-Ac) gear pumps (Liquiflo). When generating concentration waves care was taken to maintain a constant total volume flow of the two phases, as is assumed in the theory. The water was ordinary tap water; no special treatment was given to remove surfactants. The set-up has been operated with co-current and counter-current flow, with superficial liquid velocities ranging from -0.04 to $+0.18$ m s^{-1} and gas volume concentrations up to 45%.

5.2. *Measurement of bubble size*

The bubble size is measured by sucking bubbles out of the flow into a glass capillary with accurately known inner diameter. In the capillary the bubbles are stretched into long slugs, that are forced to move past two optical sensors. When a slug passes a sensor this will give a block pulse; from the time lag between the pulses and the duration of the pulses the slug length can be calculated. The equivalent bubble diameter appeared to increase with the gas flow rate (and so with the volume fraction): from 2.8 mm to 4.2 mm, with a constant variance of about 0.6 mm.

5.3. *Measurement of gas volume concentration and mean bubble velocity*

The mean volume concentration under steady flow conditions is determined by measuring the pressure drop over a short distance (12.5 cm) along the pipe with inverted U-tube Betz-manometers (van Essen). The level difference inside the U-tubes is a measure of the volume concentration.

Estimates of the local values of the volume concentration and the mean bubble velocity, again under steady conditions, are obtained by means of optical probes (Photonetics), introduced into the flow at 3.35 m above the inlet of the pipe. These probes consist of two optical fibres with a diameter of 25 μm with a sharp tip of 15 μm, placed a distance of 1.8 mm apart. The output of the probes is two trains of block pulses; the volume concentration is deduced from the duration of the pulses and the mean bubble velocity from the time lag between the bubbles. The measured volume fraction is very sensitive to the discriminator level used to distinguish between the water and the gas phase: e.g. averaging the local volume concentration over the cross-section always gave lower values, relatively 10%, than found with the Betz-manometers. Errors also occur when determining the mean bubble velocity, so that the volume concentration and mean bubble velocity profiles shown in figure 12 (§8) only give qualitative information.

The measurements with the optical fibre probes show that as long as the flow is not turbulent, the volume concentration and the mean bubble velocity are nearly uniform over the cross-section of the pipe. Therefore the mean bubble velocity can be obtained accurately from measurements of the mean volume concentration. If $\dot{m}_g$ and $\dot{m}_l$ denote the mass flow rates of gas and liquid respectively, and the diameter of the tube is D, then the mean bubble velocity in a zero-volume flux frame is given by

$$U(\phi) = \frac{1-\phi}{(\pi/4)D^2}\left(\frac{\dot{m}_g}{\rho_g \phi} - \frac{\dot{m}_l}{\rho_l(1-\phi)}\right). \tag{5.1}$$

The local gas density is determined from the pressure drop in the pipe, by assuming that the gas behaves isothermally.

5.4. *Detection of volume concentration waves*

The concentration waves are recorded by four impedance probes at 0.87 m, 2.04 m, 3.22 m, and 4.47 m above the inlet of the pipe; the probes were newly designed and differ from those used by van Wijngaarden & Kapteyn (1990). A probe consists of two 1 mm thick stainless steel measuring electrodes of 90° arc and 1.6 cm height, shielded by two pairs of similar electrodes that are isolated from the measuring electrodes by buffer amplifiers. The latter ensure that the voltage difference over the pairs of shielding electrodes is equal to that over the measuring electrodes; in this way a good sensitivity to axial concentration disturbances is achieved. Details of the electric circuit are given in Lammers (1994). A measuring electrode forms part of a Wheatstone bridge, in which it is placed in the same branch as a variable resistor that serves to balance the bridge. The bridge is operated with a carrier frequency of 5 kHz and an input voltage of 0.5 V. The resistor value of the bubbly fluid, R_x, is nonlinearly dependent on the volume concentration. On the other hand, the bridge output voltage U_x depends nonlinearly on the resistor value:

$$U_x = \hat{U}\left(\frac{R_x}{R_x - R_v} - \frac{R_1}{R_1 + R_2}\right);$$

here $\hat{U}$ denotes the input voltage, the resistor values of the fixed branches are R_1 and R_2, and that of the balancing branch is R_v. If it is assumed that the effective conductivity of the bubbly fluid σ depends on the volume concentration according to von Bruggeman's relation $\sigma = \sigma_l(1-\phi)^{3/2}$, with σ_l the conductivity of the fluid, then this would imply that the nonlinearities cancel exactly with the choice of a resistor ratio of 1:5 in the fixed branch of the bridge. This would yield a measuring system with a linear response, i.e. with $\{\partial^2 U_x/\partial\phi^2\}_{U_x=0} = 0$. Calibration with a Betz-manometer showed that this was indeed the case.

The output signals of the Wheatstone bridges are filtered by low-pass filters (KEMO) that give virtually no signal distortion when not very close to the cut-off frequency, which was typically 8 Hz to 10 Hz. An industrial PC was used for control and storage of raw data, analysis being done off-line.

From measurements with cubic arrays of polystyrene spheres van Wijngaarden & Kapteyn (1990) deduced that their impedance probes had a step response of

$$\phi_m(t) = \tfrac{1}{2}\phi_s(1 + \tanh sy)$$

with $s = 115\ \mathrm{m}^{-1}$; ϕ_s is the amplitude of the imposed signal and $y = x - ct$, with c the wave speed. This means that the response $I(k)$ for a wave component with wavenumber k is

$$I(k) = \frac{k\pi}{2s\sinh(k\pi/2s)},$$

which for long waves can be approximated by

$$I(k) \simeq 1 - \frac{\pi^2}{24}\left(\frac{k}{s}\right)^2.$$

For wavelengths larger than 12.5 cm ($k < 50\ \mathrm{m}^{-1}$), as in our experiments, the deviation from unity would be less than 8%. For more general wave shapes one estimates that the detected signal behaves as

$$\phi_m(t) = \phi(y) + \frac{\pi^2}{24s^2}\frac{\mathrm{d}^2\phi}{\mathrm{d}y^2}. \tag{5.2}$$

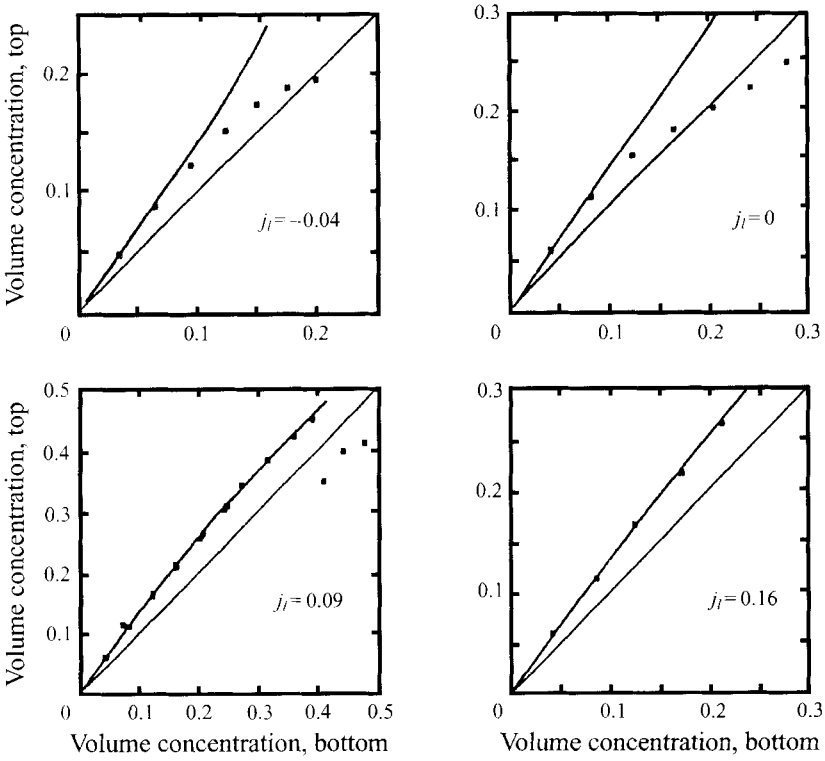

FIGURE 2. Longitudinal variation of the mean volume concentration for various superficial liquid velocities j_l; ■, experiments; —, model. The distance between 'bottom' and 'top' is 4.35 m; the values of j_l are in m s^{-1}.

For the original bridge system of van Wijngaarden & Kapteyn (1990) most of the signal distortion is associated with the tail of the response function, and was caused by cross-talk between the measuring electrodes and shielding electrodes. Their work was concerned with rather thin shock waves; using (5.2) the distortion of a concentration shock wave with thickness of e.g. 5 cm can be estimated as 10%. We performed experiments on much weaker shocks with thickness in the range 5–20 cm; and since our improved design of the bridge circuit eliminates the tail of the response function, this justifies the neglect of distortion when analysing the data.

5.5. *Longitudinal variation of the volume concentration*

For the calibration of the impedance probes during experimental runs (to check on runaway of the bridge system) it is useful to have a model which allows a calculation of the longitudinal concentration variation from a measurement with a Betz-manometer at just one location. This model follows from the condition that the mass flux of gas is constant, i.e. $\mathrm{d}\dot{m}_g/\mathrm{d}x = 0$. Differentating (5.1), and using

$$\frac{\mathrm{d}\rho_g}{\mathrm{d}x} = \frac{1}{\mathscr{R}T}\frac{\mathrm{d}p_l}{\mathrm{d}x} = -\frac{\rho_l(1-\phi)g}{\mathscr{R}T},$$

where $\mathscr{R}$ denotes the gas constant and T the temperature, yields

$$\frac{\mathrm{d}\phi}{\mathrm{d}x} = \frac{(\pi/4)D^2[\rho_l(1-\phi)g/\mathscr{R}T]\phi^2(j_l+U)^2}{\dot{m}_g[j_l+U+\phi(1-\phi)\mathrm{d}U/\mathrm{d}\phi]}. \tag{5.3}$$

Here $j_l = 4\dot{m}_l/\rho_l \pi D^2$ is the superficial liquid velocity. Once a relationship for $U(\phi)$ is determined from experiments, equation (5.3) can be integrated numericallly to obtain $\phi(x)$, if the concentration at one particular location is specified. Examples are shown in figure 2, where measured values of the volume concentration for four different flow rates are compared with calculations from a specification of the volume concentration just above the pipe inlet. To exemplify the longitudinal variation more clearly the bisector is also drawn. The model works well up to the point where the flow instability sets in.

6. Experimental procedure

The increase in gas volume concentration along the pipe can be accounted for in the theory by replacing the right-hand side of (1.1) by a term $\lambda\phi V$, with λ defined as $\lambda = -(1/\rho_g)\mathrm{d}\rho_g/\mathrm{d}x$. The weakly nonlinear wave equation then becomes the generalized Burgers equation

$$\frac{\partial \phi'}{\partial x} + \left(\frac{1}{c_0} - \frac{c_1}{c_0^2}\phi'\right)\frac{\partial \phi'}{\partial t} = \frac{\mathscr{D}}{c_0^3}\frac{\partial^2 \phi'}{\partial t^2} + \lambda\phi'. \tag{6.1}$$

The strength of the source term can be estimated from the relation

$$\lambda = -\frac{1}{\rho_g}\frac{\mathrm{d}\rho_g}{\mathrm{d}x} = -\frac{1}{p_l}\frac{\mathrm{d}p_l}{\mathrm{d}x},$$

which yields a typical value

$$\lambda = \rho_l g(1-\phi)/p_l \simeq 10^3 \times 10 \times 0.88/1.3 \times 10^5 \simeq 0.07\ \mathrm{m}^{-1}.$$

Whether the propagation of long, weakly nonlinear concentration waves is governed by the generalized Burgers equation (6.1) has been examined by comparing the evolution of imposed concentration disturbances with solutions to this equation. The comparison was done by a fit procedure with the velocities c_0 and c_1 and the diffusivity $\mathscr{D}$ (for periodic disturbances), or c_0 and the combination $c_1/\mathscr{D}$ (for step-like disturbances), as free parameters. This lead to excellent matches between the calculated and the recorded wave profiles, and to a consistent set of values for the free parameters, so it effectively was a method of measuring the diffusivity $\mathscr{D}$.

6.1. *Periodic concentration waves*

The propagation of sinusoidal finite-amplitude disturbances has been studied for superficial liquid velocities in the range -0.04 to 0.16 m s^{-1} and for mean volume concentrations up to 32%. For measuring of the diffusivity $\mathscr{D}$ data analysis was performed on nine time series, with four different imposed frequencies and amplitudes. From each time series 64 wave cycles were taken, and 128 points per cycle; the sampled signal of an electrode was then used as a boundary condition in a numerical calculation of the wave evolution by a pseudo-spectral method with 1024 harmonics, and the result subsequently 'compared' with the spectral decomposition of the sampled signal of the next electrode higher-up: i.e. with an iteration procedure that uses the source frequency and a few harmonics (typically 4), values for the diffusivity $\mathscr{D}$ and the velocities c_0 and c_1 are calculated that give the best fit for all nine time series. Further details may be found in Lammers (1994).

We have also done calculations with a dispersive term added to the wave equation, with the dispersion coefficient as an additional free parameter in the fit procedure, but were not able to obtain a definite value for this very small coefficient. The structure

of the shocks that form within the periodic waves show hardly any asymmetry, which also indicates that dispersive effects are not pronounced.

6.2. *Concentration shock waves*

The effects of bubble growth can be neglected when analysing the structure of concentration shock waves. It follows from Burgers' equation that upon step-wise lowering of the gas flow rate a concentration shock wave (an expansion shock) will form after a time of the order $16\mathscr{D}/(c_1(\phi_1 - \phi_2))^2$, with a structure described by

$$\phi(x,t) = \frac{\phi_1 + \phi_2}{2} + \frac{\phi_2 - \phi_1}{2} \tanh \frac{c_1(\phi_2 - \phi_1)(x - U_S t)}{4\mathscr{D}}. \tag{6.2}$$

Here ϕ_1 is the volume fraction in front of the shock, ϕ_2 that behind ($\phi_1 > \phi_2$); c_1 and $\mathscr{D}$ are to be evaluated for the mean volume concentration $\phi_m = \frac{1}{2}(\phi_1 + \phi_2)$, and the shock speed is given by

$$U_S = c(\phi_m) + \phi_m \left\{ \frac{\mathrm{d}c}{\mathrm{d}\phi} \right\}_{\phi=\phi_m}.$$

For experimental verification it is convenient to define the shock-wave thickness Δ_S as the distance between the points where the tangent line through the inflection point crosses the levels ϕ_1 and ϕ_2, giving

$$\Delta_S = \frac{8\mathscr{D}}{c_1(\phi_2 - \phi_1)}. \tag{6.3}$$

All experiments on concentration shock waves were performed with stagnant water. A good impression of the shock profile could be obtained by averaging the recordings of 80 runs. First the volume concentrations far in front of and far behind the shock wave were determined for each recording; these were subsequently 'centred' by requiring that the recorded profiles cut out equal areas between horizontal lines at the upper and lower levels, and then the averaging was carried out. Next, a best fit to the Taylor solution (6.2) was obtained by a numerical method that uses $c_1/\mathscr{D}$ as a free parameter, and a value of the shock speed U_S determined by a comparison between the recordings at two measuring stations. The diffusivity $\mathscr{D}$ then followed by calculating $c_1 = \mathrm{d}c_0/\mathrm{d}\phi$ from the experimentally determined relation (7.1) given below.

7. Experimental results for concentration waves

7.1. *Small-amplitude disturbances*

Measured values of the mean bubble velocity and the speed of small-amplitude concentration waves for various liquid flow rates are shown in figure 3; these fit onto a single curve when expressed with respect to a zero-volume-flux reference frame. A correlation of the form (4.1) yields $U_\infty = 21.4$ cm s^{-1} and $p = 1.70$. For single bubbles with an equivalent diameter of approximately 3.5 mm, rising in tap water, Haberman & Morton (1953) measured velocities of about 23 cm s^{-1}; values of p between 1.5 and 2.3 are commonly found for bubbly flows in pipes. To verify the relationship between the kinematic wave speed and the velocity of the bubbles a polynomial fit of the wave speed measurements is first made:

$$c_0(\phi) = 0.219(1 - \phi)(1 - 3.08\phi + 2.77\phi^2 - 0.55\phi^3), \tag{7.1}$$

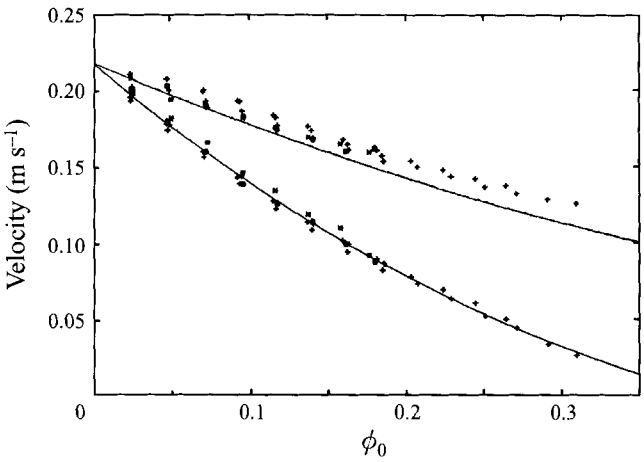

FIGURE 3. Measured values of the mean bubble velocity (upper set of points) and linear concentration wave velocity (lower set of points) as a function of the gas volume concentration ϕ_0. The data were obtained for superficial liquid velocities of -0.04, 0.00, 0.04, 0.08 and 0.14 m s^{-1}; the data are expressed with respect to a zero-volume-flux reference frame. The lower solid curve is a fit through the wave velocity data; the upper solid curve is obtained from this fit by using equation (2.4).

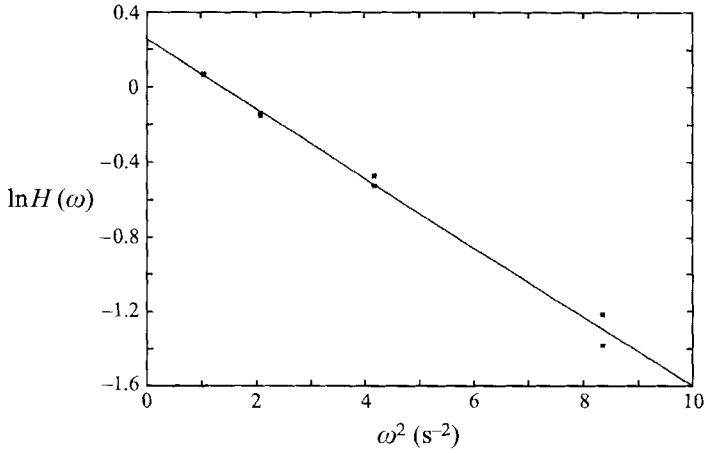

FIGURE 4. Attenuation as a function of the frequency ω of small-amplitude concentration waves over a distance of 4.46 m in a bubbly flow with a mean volume concentration of 10%. The attenuation is well represented by the transmission function $H(\omega)$ given in relation (7.2).

and then relation (2.4) is integrated, which gives

$$U(\phi) = 0.219(1 - \phi)(1 - 1.0\phi + 0.55\phi^2).$$

The fit (the lower solid curve) and the result of the integration (the upper solid curve) are shown in figure 3.

Data for the damping of small-amplitude waves over a distance of 3.6 m are presented in figure 4; here $\phi_0 = 10\%$. From equation (6.1) it follows that the relation between the attenuation and the angular frequency ω can be expressed by a transmission function

$$H(\omega) = \exp\left(\lambda - \frac{\mathscr{D}\omega^2}{c_0^3}\right) x. \tag{7.2}$$

Figure 4 confirms that $\ln H$ is a linear function of ω^2. The value of $\ln H$ on the abscissa corresponds to $\lambda = 0.07$ m^{-1}, which is equal to the estimate given in the previous section; the slope of the line yields a diffusivity of $\mathscr{D} = 2.7 \times 10^{-4}$ m^2 s^{-1}.

7.2. *Periodic finite-amplitude waves*

To examine the propagation of sinusoidal finite-amplitude disturbances it is useful to rewrite (6.1) in variables made dimensionless with the frequency ω and amplitude ϕ_s of the source-signal. By introducing

$$\theta = \omega\left(t - \frac{x}{c_0}\right), \quad z = \frac{\omega\phi_s|c_1|}{c_0^2}\int_0^x \exp\left(\int_0^{x'} \lambda \mathrm{d}x''\right)\mathrm{d}x',$$

$$\phi^* = \frac{\phi'}{\phi_s}\exp\left(-\int_0^x \lambda \mathrm{d}x'\right), \quad \nu = \frac{\omega\mathscr{D}}{c_0|c_1|\phi_s}\exp\left(-\int_0^x \lambda \mathrm{d}x'\right)$$

the canonical form

$$\frac{\partial\phi^*}{\partial z} - \phi^*\frac{\partial\phi^*}{\partial\theta} = \nu(z)\frac{\partial^2\phi^*}{\partial\theta^2} \tag{7.3}$$

of the generalized Burgers equation obtained (Nimmo & Crighton 1986). The use of the symbol θ here as well is standard, and will cause no confusion. The above formulation shows that the behaviour of solutions of the generalized Burgers equation (and thus the propagation of nonlinear acoustic waves) can be studied from experiments on volume concentration waves in a pipe of fixed length by varying the frequency and the amplitude of the source signal, and, since (6.1) is defined with respect to a zero-volume-flux frame, by varying the superficial liquid velocity.

Some examples of the recorded wave evolution and that obtained by a numerical calculation using the sampled wave profile at the lowest measuring station as boundary value, are shown in figure 5. The 'wiggly' solid lines are the recorded wave shapes at (from top to bottom) 0.87 m, 2.04 m, 3.22 m, and 4.47 m above the inlet of the pipe; the dashed lines are the calculated waves. Note that in order to represent everything in a single figure the recordings of the three upper stations have been shifted in phase. In all these examples the superficial liquid velocity is 0.03 m s^{-1} and the mean gas volume concentration at the lowest station is 6%. The imposed wave periods are, 4.352 s (*a,d*), 3.072 s (*b,e*) and 2.176 s (*c,f*); the imposed signal amplitudes are 1.5% (*a–c*) and 2.0% (*d–f*). Note that for a clear presentation we chose signal amplitudes that are strictly speaking too large for the theory to apply. Nevertheless the examples show some of the behaviour typical for the Burgers equation. For a fixed signal strength the frequency increases from top to bottom, giving rise to stronger diffusive effects and less-pronounced nonlinear steepening. From left to right the signal strength increases for a fixed frequency; the nonlinear effects become more prominent, and so the wave shapes become steeper. In figures 5(*d*) and 5(*e*) a shock is formed between the first and second station. In figures 5(*c*) and 5(*f*) the wave amplitudes at the upper measuring station have become nearly independent of the signal amplitude; the wave profiles are typical for waves in the final stages of decay.

The resemblence of the wave evolution to the familiar features of the sinusoidal signalling problem for the 'ordinary' Burgers equation with small ($\nu \ll 1$), constant diffusivity (Crighton & Scott 1979; Crighton 1992), can be seen even more clearly in the second set of examples given in figure 6. For these recordings the parameter values have been chosen so that the bubble growth effects are unimportant. The

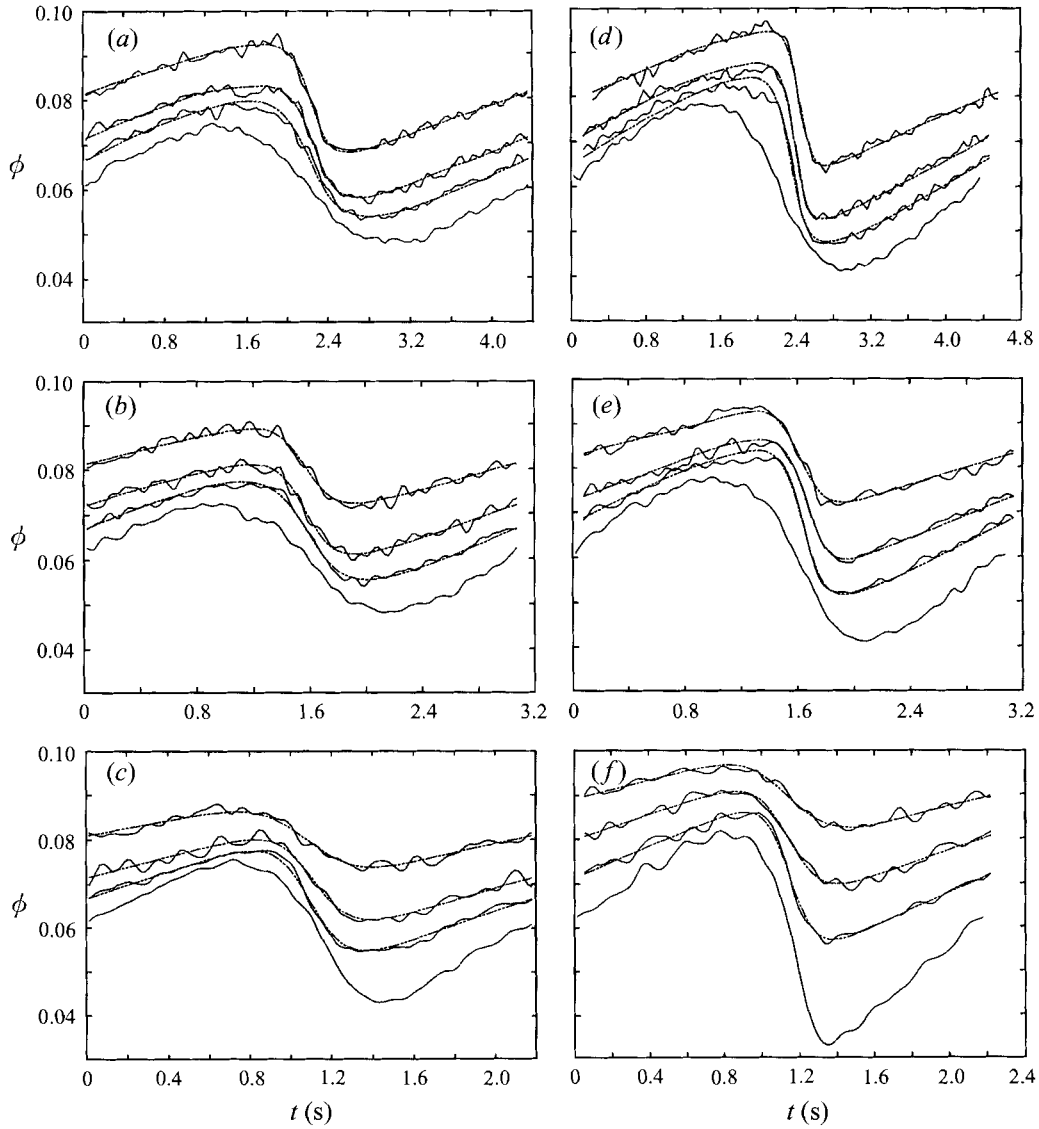

FIGURE 5. Examples of the evolution of sinusoidal finite-amplitude concentration disturbances. The wiggly solid curves are the wave profiles recorded at (from top to bottom) 0.87 m, 2.04 m, 3.22 m, and 4.47 m above the inlet of the pipe. The last three profiles have been shifted in order to present them in a single figure. The dashed curves are numerically calculated solutions of the generalized Burgers' equation with the sampled signal at 0.87 m as boundary condition. In each case the superficial liquid velocity is 0.03 m s^{-1}, and the mean volume concentration is 6%. Wave periods are 4.352 s (*a*,*d*), 3.072 s (*b*,*e*) and 2.176 s (*c*,*f*); signal amplitudes are 1.5% (*a*–*c*), 2.0% (*d*–*f*).

'operating conditions', i.e. the values for the superficial liquid velocity j_l, the mean volume concentration at the inlet of the pipe ϕ_0, the signal amplitude ϕ_s, and the wave period T, are given in the first four columns of table 1. The measured values of the diffusivity $\mathscr{D}$ and the wave velocities c_0 and c_1 are given in the next three columns of table 1, whereas the last five columns give values of the dimensionless parameters v and z; the lowest measuring station is at z_1 and the highest at z_4.

In figure 6(*a*) the sinusoidal wave develops into a sawtooth wave with profile

	j_l m s^{-1}	ϕ_0 (%)	ϕ_s (%)	T (s)	$\mathscr{D}$ (10^{-3} m^2 s^{-1})	c_0 (m s^{-1})	c_1 (m s^{-1})	ν	z_1	z_2	z_3	z_4
Figure 6(*a*)	−0.03	7.0	5.4	15.4	0.25	0.140	−0.80	0.017	0.80	1.88	2.96	4.11
Figure 6(*b*)	−0.03	8.0	5.0	2.56	0.21	0.136	−0.75	0.10	4.39	10.15	16.02	

TABLE 1. The flow parameters for figure 6

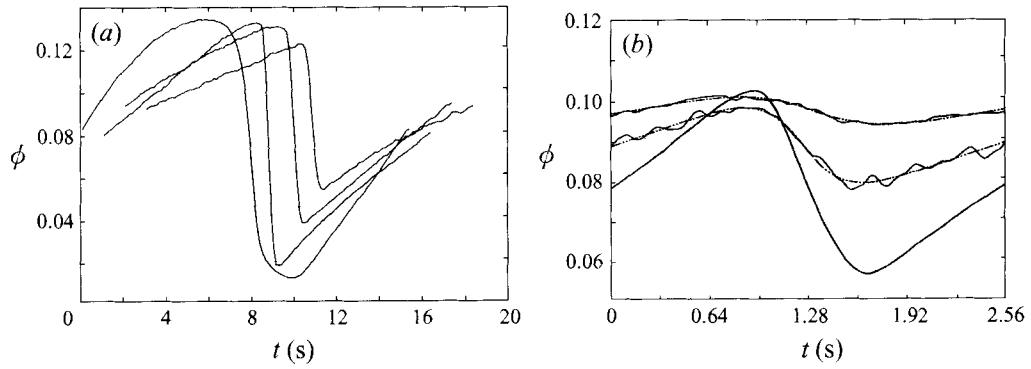

FIGURE 6. Examples of the evolution of sinusoidal finite-amplitude concentration disturbances, illustrating (*a*) formation and decay of a sawtooth wave, (*b*) the wave entering the old-aged sinoid regime. The wiggly solid curves are the wave-profiles recorded at (from left to right) 0.87 m, 2.04 m, 3.22 m, and 4.47 m (only in *a*) above the inlet of the pipe. The last profiles have been shifted in order to present them in a single figure. The dashed curves in (*b*) are numerically calculated solutions of the generalized Burgers' equation with the sampled signal at 0.87 m as boundary condition. Values of the flow parameters are given in table 1.

approximately described by

$$\phi' \simeq \phi_s \frac{\pi - \theta}{z} = \frac{c_0^2}{\omega c_1 x}\left(\pi - \omega(t - x/c_0)\right)$$

that has internal shocks

$$\phi' \simeq \phi_s \frac{\pi}{z} \tanh\left(\frac{\pi\theta}{2\nu z}\right) = \frac{\pi c_0^2}{\omega c_1 x} \tanh \frac{\pi c_0^3 (t - x/c_0)}{\omega \mathscr{D}},$$

with strength $4\pi c_0^2/\omega c_1 x$ and thickness $4\omega\mathscr{D}x/\pi c_0^2$. Ultimately the shocks decay, and figure 6(*b*) shows the formation of an 'old-aged sinoid', a small-amplitude sinusoidal wave described by

$$\phi' \sim 4\nu\phi_s e^{-\nu z} \sin\theta = \frac{4\mathscr{D}\omega}{c_0 c_1} e^{-(\omega^2\mathscr{D}/c_0^3)x} \sin\omega(t - x/c_0).$$

Both the sawtooth wave and the old-aged sinoid have an amplitude that is independent of the source amplitude.

The phenomenon that with increasing strength of the source signal the amplitude of the signal recorded at a point sufficiently far from the source becomes independent of the source strength ('amplitude saturation') is exemplified further in figure 7. These data were obtained at a single measuring station (station 4 in 7(*a*), station 3 in 7(*b*)) by varying the source strength while all other flow parameters were kept fixed (which implies that νz has constant value). The encircled points correspond to the curves on the right in figures 6(*a*) and 6(*b*), so that information on the flow parameters can be

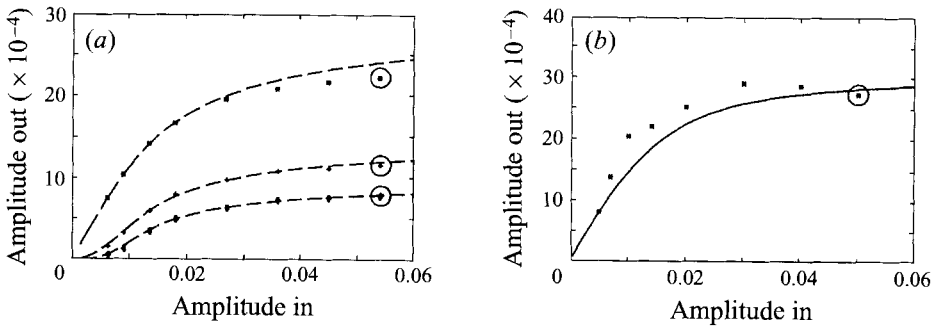

FIGURE 7. (*a*) Amplitude saturation in the sawtooth-wave regime, illustrated for the first three harmonics of a Fourier series representation of the wave profile. The encircled data correspond to the wave profile at 4.47 m shown in figure 6(*a*). (*b*) Amplitude saturation in the old-aged sinoid regime. The encircled point corresponds to the wave-profile at 3.22 m shown in figure 6(*b*). The dashed curves in both figures are obtained from approximate analytical solutions given in the text.

found in the caption of these figures. Figure 7(*a*) shows how the recorded amplitudes of the first three harmonics of a Fourier series representation of the signal vary as a function of the source amplitude. The dashed curves have been calculated from a Fourier series representation of the solution of the generalized Burgers equation for small values of ν, essentially by matching the Blackstock solution (Blackstock 1966) to a Fourier series represenation of the solution for the 'embryo-shock' region given by Lighthill (1956, §8.3), to overcome the singularity at $z = 1$ in an expansion of the amplitude in terms of ν. Figure 7(*b*) shows the variation with the signal amplitude of the recorded amplitude of waves in the old-aged sinoid regime. In this case the solid curve has been calculated from the solution of Cole (1951), corrected for bubble growth effects, i.e.

$$\phi' \simeq 4\nu\phi_s \frac{I_1(1/2\nu)}{I_0(1/2\nu)} \, \mathrm{e}^{(\lambda-\omega^2\mathscr{D}/c_0^3)x} \sin\omega(t - x/c_0).$$

$I_n(x)$ is the modified Bessel function. As far as we know amplitude saturation of planar nonlinear acoustic waves in the old-aged sinoid stage of development has not been demonstrated experimentally before.

7.3. *Concentration shock waves*

Two examples of recordings of concentration shock waves (expansion shocks), together with fits based on the Taylor solution, are given in figure 8. Data for the shock thickness as a function of the shock strength are presented in figure 9; the mean volume concentration is 9.7% in all cases. Clearly the thickness is inversely proportional to the strength, as it should be.

We now confirm that the conditions $F \ll 1$ and $R \gg 1$, on which the derivation of the Burgers equation in §2 was based, are satisfied in the experiments. An extreme case is a concentration shock wave with strength $\phi_1 - \phi_2 = 0.125 - 0.075$ in a bubbly flow with mean volume concentration of 10%. The observed shock thickness is approximately 5 cm, which is sufficiently large compared to the bubble radius, $a \simeq 0.2$ cm, to allow a continuum approach. The shock speed is $U_S \simeq 12.5$ cm s^{-1}, which yields a time scale $T \simeq \Delta_S/U_S \simeq 0.4$ s. A crude estimate of the added mass coefficient is $C = 1.8$ and the mean velocity of rise of the bubbles is inferred from figure 3 to be about $U_0 = 0.18$ m s^{-1}. Thus $F \simeq CU_0/\gamma gT \simeq (1.8 \times 0.18)/(1 \times 10 \times 0.4) \simeq 0.08$, and $R^{-1} \simeq \beta(a/CU_0T) \simeq \beta(0.002/1.8 \times 0.18 \times 0.4) \simeq 0.02\beta$. Both numbers are small

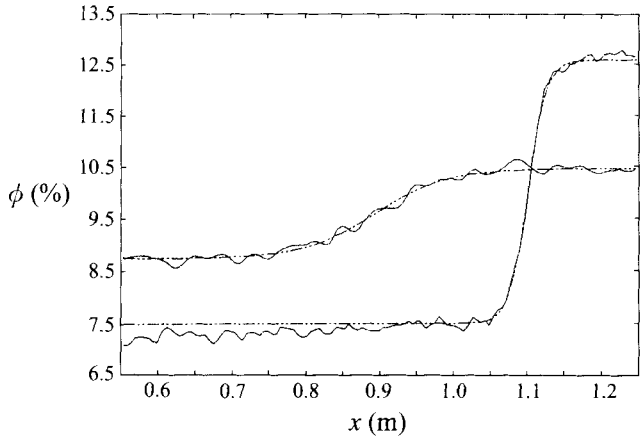

FIGURE 8. Two examples of recorded concentration shock wave profiles (the wiggly solid curves) and numerical fits based on the Taylor shock solution (the dashed curves). The mean volume concentration is 9.7%; shock strengths are 1.65% and 5.1%, shock thicknesses are 18.8 cm and 5.0 cm respectively.

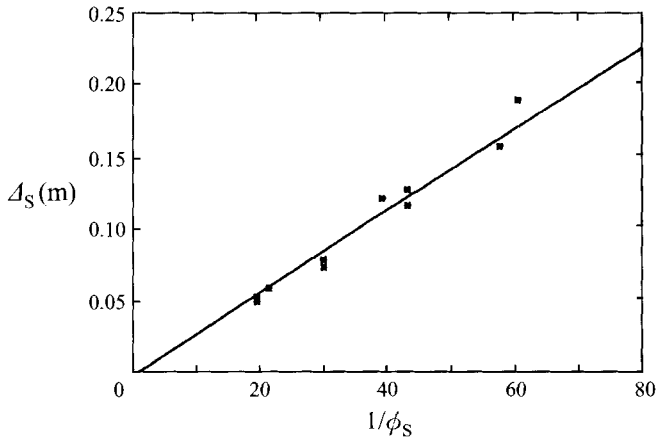

FIGURE 9. Data confirming that the thickness Δ_S of concentration shock waves is inversely proportional to the shock strength $\phi_S = \phi_1 - \phi_2$. The mean volume concentration $(\phi_1 + \phi_2)/2$ is 9.7% in each case.

for values of β of order one. These estimates also confirm that the scalings used in the derivation of evolution equations for weakly nonlinear unstable waves in §3 are appropriate.

7.4. *Diffusivity of concentration waves*

Values of the velocity c_1 and the diffusivity $\mathscr{D}$ obtained from experiments on nonlinear periodic waves for volume concentrations up to the critical value, have been collected in figures 10(*a*) and 10(*b*) respectively. These were calculated from samples of the recordings at the measuring stations 2.04 m and 3.22 m above the inlet. In the figures the number 0 corresponds to measurements with stagnant water, the numbers 4 and 8 to superficial liquid velocities of 0.04 and 0.08 m s^{-1}, and + indicates a superficial liquid velocity of 0.16 m s^{-1}. Figure 10(*b*) also includes data obtained from shock wave experiments in stagnant liquid; these are marked with an S. For comparison a solid line calculated from $c_1 = dc_0/d\phi$ using the fit (7.1) is drawn in figure 10(*a*).

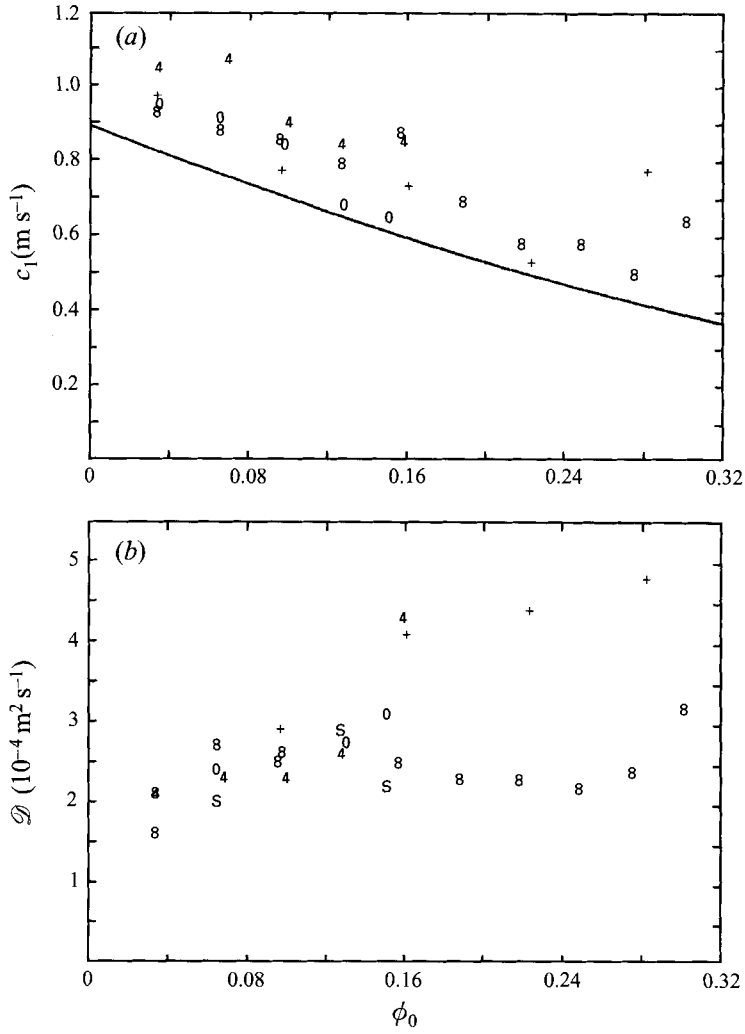

FIGURE 10. Values of the velocity c_1 (*a*) and the diffusivity $\mathscr{D}$ (*b*) determined from experiments on weakly nonlinear concentration waves. The data marked by 0, 4, 8, and + are for sinusoidal disturbances in flows with a superficial liquid velocity 0, 4, 8, and 16 m s^{-1} respectively; the data marked by S are from concentration shock wave experiments in stagnant liquid. The solid line in (*a*) is calculated from a fit through data for the velocity of small-amplitude waves (the lower solid curve in figure 3).

The diffusivity $\mathscr{D}$ is found to be of order 2.5 10^{-4} m^2 s^{-1}. The non-dimensional diffusivity $\mathscr{D}/a|U|$ is of the order 0.3 to 0.5, and as explained in §4 this is also an estimate of the value of α. The diffusivity is markedly higher in the experiments with a superficial liquid velocity of 0.16 m s^{-1}. The most likely explanations are that turbulence in the liquid phase and non-uniformity of the mean mixture parameters over the cross-section enhance the 'diffusive' effects.

8. Experiments on the onset of flow transition

We now describe some observations of the onset of transition from uniform bubbly flow to turbulent bubbly flow.

Figure 11 shows how the relationship between the mean velocity of rise of the

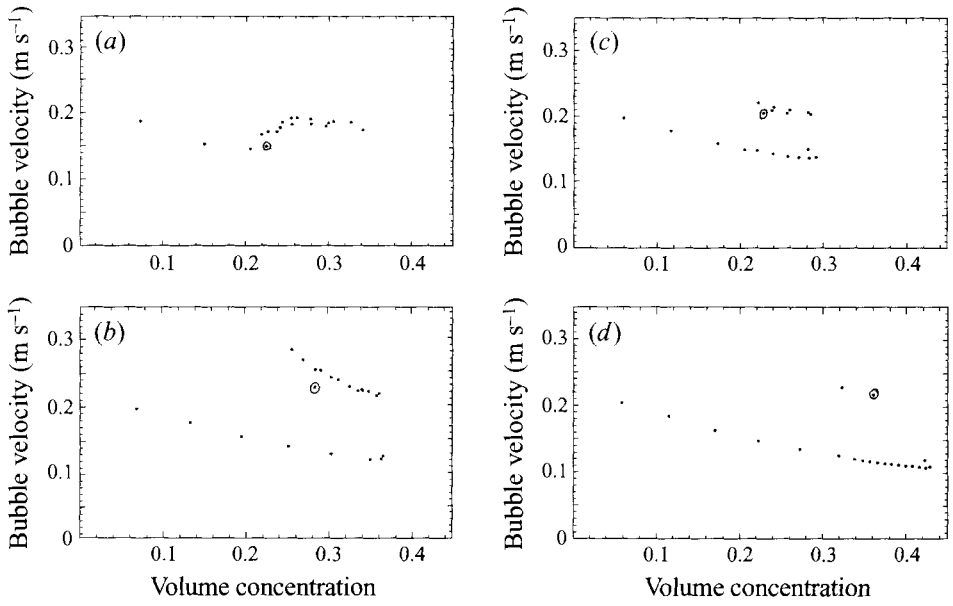

FIGURE 11. The change in the relationship between the mean bubble velocity and the mean gas volume concentration as the homogeneous bubbly flow becomes turbulent. In a turbulent flow the mean bubble velocity is larger for a given value of the volume concentration. Measurements at 4.97 m (*a,b*) and 2.97 m (*c,d*) above the pipe inlet, and for two liquid flow rates: stagnant water (*a,c*) and superficial liquid velocity $j_l = 0.08$ m s^{-1} (*b,d*). The encircled data are for the case in which the flow transition occurs a little below the measuring station.

bubbles, relative to a zero-volume-flux reference frame, and the mean gas volume concentration changes as the bubbly flow becomes turbulent. Presented here are measurements for two liquid flow rates, stagnant liquid (*a,c*) and superficial liquid velocity 0.08 m s^{-1} (*b,d*), and at two positions h along the pipe: at 2.97 m (*a,b*) and 4.97 m (*c,d*) above the pipe inlet. As mentioned before, the transition point moves downwards when the gas flow rate is increased; the encircled data in figure 11 are for the situation in which the turbulent regime of flow begins right at the measuring station, so that the corresponding value of the mean volume concentration is an indication of ϕ_c.

In the case of homogeneous bubbly flow the data for different liquid flow rates (the 'lower' set of points in figure 11) fall onto a single curve shown in figure 3; it appears from figure 11 that as the flow undergoes transition the mean gas volume concentration drops and the mean bubble velocity increases. This is because in the region of turbulent flow the bubbles form clusters which move upwards with high speed, preferably near the centreline of the pipe, whereas close to the wall the bubbles have low speed and may sometimes move downward.

Remarkable about figure 11 is that the critical value of the concentration depends on the liquid flow rate and on the distance from the bubble distributor. This is not what would be expected from Batchelor's theory, and we have no explanation for it. It is tempting to relate the discrepancy to the sensitivity of ϕ_c on the bubble size, as exemplified in figure 1 for smaller bubbles than those in the experiments. It shows that for $\alpha > 0.3$ and for non-spherical bubbles (diameters larger than 0.7 mm) the critical volume concentration increases with the bubble size. In the experiments the bubble size varies somewhat with the liquid flow rate and with the gas flow rate, smaller bubbles occurring when either of these flow rates is less. Thus if the inference

j_l m s^{-1}	h (m)	d_i (mm)	d_c (mm)
0.00	4.97	3.1	3.4
0.00	2.97	3.3	3.4
0.08	4.97	3.6	3.9
0.08	2.97	3.8	4.0

TABLE 2. The bubble diameters at the pipe inlet and at the measuring station at various heights and flow rates

that ϕ_c becomes larger with increasing size of the bubbles is correct for the bubbles in our experiments, this implies that ϕ_c should be larger in the right figures and in the lower figures; this is indeed the case. Table 2 gives the values of the bubble diameters at the pipe inlet d_i and at the measuring station d_c in the experiments that gave the encircled data in figure 11. For equal values of the height h the bubble size d_c is larger when $j_l = 0.08$ m s^{-1} than when $j_l = 0.0$ m s^{-1}, so that the above argument seems to explain why ϕ_c is larger in figures 11(b) and 11(d). On the other hand the bubble size d_c is roughly equal for the same values of j_l but different heights h, so that the argument does not answer the question why, for a given liquid flow rate, ϕ_c is less when the point of transition is higher-up in the tube. Perhaps the reason is, in terms of Batchelor's theory, that the diffusivity $\mathscr{D}$ decreases along the pipe, e.g. because the bubble velocity fluctuations diminish as the bubbles rise. We have not found other evidence for this.

Next, figure 12 shows how the radial profiles of the local volume concentration (a,b) and local mean bubble velocity in a laboratory reference-frame (c,d) change as the flow becomes unstable, for stagnant liquid (a,c) and for $j_l = 0.08$ m s^{-1} (b,d). The data were obtained with an optical probe, introduced into the flow at a height of 3.35 m above the inlet. The indicated values of the mean volume concentration are those at the inlet of the pipe, and the transition occurs, as judged by eye, approximately 1 m above (+), just above (△), and approximately 1 m below (o) the probe. What is observed is that under stable conditions (+) the bubbly flow is fairly uniform, but that just below the point of transition (△) the radial distribution (that of the gas velocity in particular) becomes of parabolic shape. This would suggest that in the initial stage of the transition there is an instability to radial disturbances rather than to planar disturbances, as is assumed in Batchelor's theory. On the other hand, what is judged by eye to be the point of transition may just as well be located a little above the point where the actual instability occurs. The parabolic profile may then be the result of a second stage of an instability to planar disturbances (see Batchelor 1993). At present there does not exist a satisfactory three-dimensional description of the dynamics of bubbly flows to settle this question; a deeper experimental investigation into the matter proved to be too difficult.

A third observation can be made from figure 10. Here it is puzzling that there is no indication of a downward trend in the diffusivity $\mathscr{D}$ as the volume concentration approaches the critical value. The explanation could be that the linearly stable flow is unstable to nonlinear disturbances: the imposed disturbances, whose propagation properties in the homogeneous flow yield the values of $\mathscr{D}$, may cause an instability to set in for values less than ϕ_c; the functional behaviour of $\mathscr{D}$ close to ϕ_c is then difficult to detect. Further analysis of the evolution equations of §3 should clarify this point.

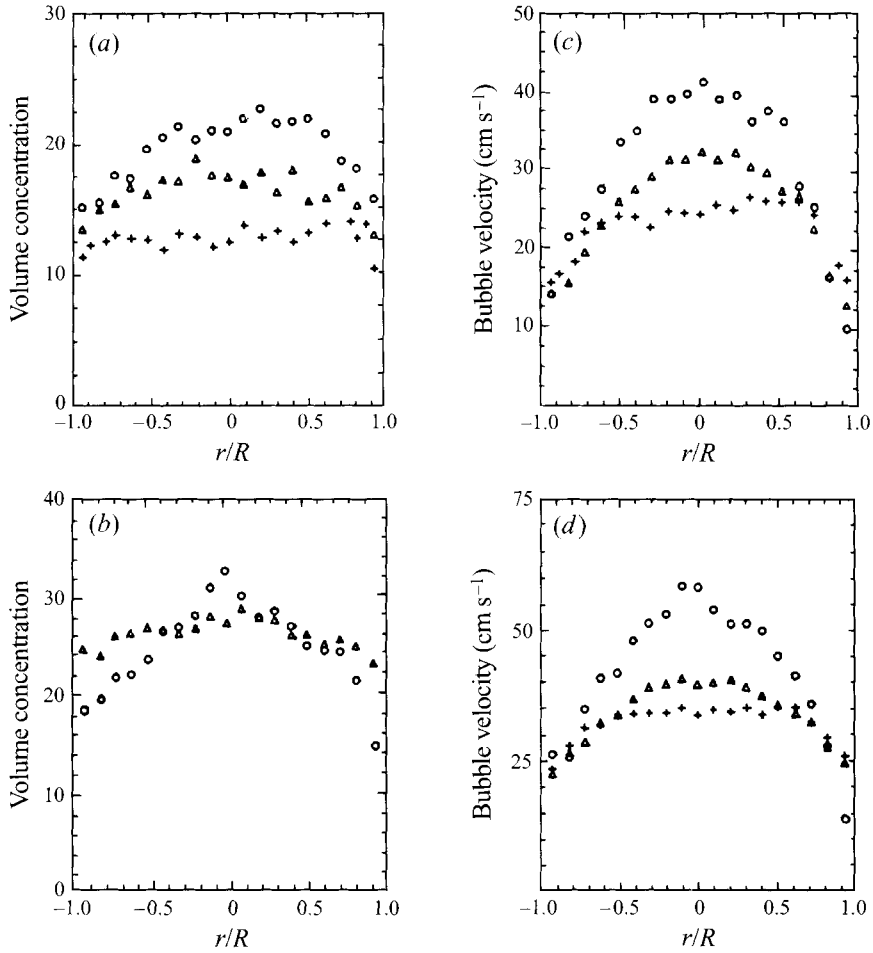

FIGURE 12. Radial profiles of the local volume concentration (*a,b*) and the local mean bubble velocity (*c,d*) close to the point of instability of a uniform bubbly flow; stagnant flow (*a,c*), superficial liquid velocity 0.08 m s^{-1} (*b,d*). Data were taken 3.35 m above the pipe inlet; the transition occurs approximately 1 m above (+), just above (△), and 1 m below (o) the measuring station. Values of the mean volume concentration at the pipe inlet, (*a,c*): 12% (+), 18% (△), 23% (o); (*b,d*): 24% (+), 28% (△), 32% (o).

9. Conclusions

We have shown that Batchelor's equations for the propagation of planar concentration disturbances in fluidized beds also apply to bubbly flows. The behaviour of long, finite-amplitude gas volume concentration waves is governed by Burgers' equation, modified by a source term that accounts for bubble growth. The observed wave profiles of expansion shock waves and periodic waves compare well with well-known solutions to Burgers' equation, and could therefore be used to measure 'the diffusivity of concentration waves'. There is evidence that for low values of the gas volume concentration (less than 10%) the dominant contribution to this diffusivity comes from the 'bulk elasticity' of the bubbles; for larger values of the concentration acceleration-reaction ('added mass') effects become important.

Batchelor's criterion for the onset of instabilities in uniform dispersions effectively says that these flows lose stability to planar concentration disturbances at a value

of the concentration for which the diffusivity becomes negative. We have derived evolution equations for the behaviour of weakly nonlinear disturbances in dispersions for which the volume concentration of the particles or bubbles is close to the critical value. These evolution equations are similar to those derived by Hayakawa *et al.* (1994), which lends support to these authors' criticism of other descriptions that have appeared in the literature.

Our observations of the onset of flow transition in bubbly flows seem to disagree with Batchelor's theory. For instance, it is found that the critical volume concentration differs with the superficial liquid velocity and the location where the instability sets in. In the experiments the bubble size changes with the liquid flow rate and the gas flow rate, and with the height in the pipe. Estimates of the parameters that determine the diffusivity of concentration waves for dispersions of small, approximately spherical bubbles suggest that the critical gas volume concentration depends strongly on the size of the bubbles, but this only partially resolves the observed discrepancy.

Batchelor (1993) explains that gas-fluidized beds are unstable to transverse disturbances as soon as they become unstable to planar disturbances. On the other hand, the experiments of El-Kaissy & Homsy (1976) and Didwania & Homsy (1981) show that in liquid-fluidized beds wave trains of considerable amplitude may develop. Our experiments suggest that in a bubbly flow the radial volume concentration profile first changes roughly from uniform into one with parabolic shape, before the bubbly flow becomes turbulent. We were unable to decide whether this change of profile is the first stage of the flow transition (thus contradicting Batchelor's 1988 theory, which assumes that a dispersion first becomes unstable to planar disturbances), or whether it is the second stage of the flow transition (as in Batchelor 1993). Wave trains of the type that have been found in liquid-fluidized beds could not be observed in our experiments; rather the uniform bubbly flow seemed to change almost at once into an agitated, kind of turbulent, flow. An analysis of what precisely happens awaits the formulation of a satisfactory three-dimensional theory; experimental verification will still be difficult because the behaviour of the flow is very sensitive to the size of the bubbles.

The authors would like to thank Earryt Boetes, Wouter den Breeijen, Henk Bulthuis, Jan-Peter Bultman, Wim Gorissen, Bettina Reinhartz, Henni Scholten, Lieuwe Seinstra, and Jaap de Wilde for their help with the experiments, and Paul Duineveld for drawing figure 1.

This work is part of the research program of the "Stichting voor Fundamenteel Onderzoek der Materie (FOM)", which is financiallly supported by the "Nederlandse organisatie voor wetenschappelijk onderzoek (NWO)". The financial support by FOM and by the Koninklijke/Shell Laboratorium, Amsterdam (KSLA) is gratefully acknowledged.

REFERENCES

BATCHELOR, G. K. 1988 A new theory of the instability of a uniform fluidized bed. *J. Fluid Mech.* **193**, 75–110.

BATCHELOR, G. K. 1991 The formation of bubbles in fluidized beds. In *Proc. Symp. Honoring John W. Miles on his 70th birthday*. Scripps Institution of Oceanography. Ref. Series 91-24.

BATCHELOR, G. K. 1993 Secondary instability of a gas-fluidized bed. *J. Fluid Mech.* **257**, 359–371.

BLACKSTOCK, D. T. 1966 Connection between the Fay and Fubini solutions for plane sound waves of finite amplitude. *J. Acoust. Soc. Am.* **39**, 1019–1026.

COLE, J. D. 1951 On a quasi-linear parabolic equation occurring in aerodynamics. *Q. Appl. Maths* **9**, 225–236.

CRIGHTON, D. G. 1992 Nonlinear acoustics. In *Modern Methods in Analytical Acoustics* (ed. D. G. Crighton), pp. 684–670. Springer.

CRIGHTON, D. G. & SCOTT, J. F. 1979 Asymptotic solutions of model equations in nonlinear acoustics. *Proc. R. Soc. Lond.* A **292**, 101–134.

DIDWANIA, A. K. & HOMSY, G. M. 1981 Flow regimes and flow transitions in liquid fluidized beds. *Intl J. Multiphase Flow* **7**, 563–580.

DIDWANIA, A. K. & HOMSY, G. M. 1982 Resonant sideband instabilities in wave propagation in fluidized beds. *J. Fluid Mech.* **122**, 433–438.

DUINEVELD, P. C. 1994 Bouncing and coalescence of two bubbles in water. PhD thesis, University of Twente.

EL-KAISSY, M. M. & HOMSY G. M. 1976 Instability waves and the origin of bubbles in fluidized beds. Part 1: Experiments. *Intl J. Multiphase Flow* **2**, 379–395.

GANSER, G. H. & DREW, D. A. 1990 Nonlinear stability analysis of a uniformly fluidized bed. *Intl J. Multiphase Flow* **16**, 447–460.

HABERMAN, W. L. & MORTON, R. K. 1953 An experimental investigation of the drag and shape of air bubbles rising in various liquids. *David Taylor Model Basin Rep.* 802.

HARRIS, S. E. & CRIGHTON, D. G. 1994 Solitons, solitary waves, and voidage disturbances in gas-fluidized beds. *J. Fluid Mech.* **266**, 243–276.

HAYAKAWA, H., KOMATSU, T. S. & TSUZUKI, T. 1994 Pseudo-solitons in fluidized beds. *Physica* A **204**, 277–289.

KYNCH, G. J. 1952 A theory of sedimentation. *Trans. Faraday Soc.* **48**, 166–176.

LAMMERS, J. H. 1994 The stability of bubbly flows. PhD thesis, University of Twente.

LIGHTHILL, M. J. 1956 Viscosity effects in sound waves of finite amplitude. In *Surveys in Mechanics* (ed. G. K. Batchelor & R. M. Davies), pp. 250–351. Cambridge University Press.

LIU, J. T. C. 1983 Nonlinear unstable wave disturbances in fluidized beds. *Proc. R. Soc. Lond.* A **389**, 331–347.

MOORE, D. W. 1965 The velocity of rise of distorted gas bubbles in a liquid of small viscosity. *J. Fluid Mech.* **23**, 749–766.

NIMMO, J. J. C. & CRIGHTON, D. G. 1986 Geometrical and diffusive effects in nonlinear acoustic propagation over long ranges. *Phil. Trans. R. Soc. Lond.* A **320**, 1–35.

WHITHAM, G. B. 1974 *Linear and Nonlinear Waves.* Wiley & Sons.

WIJNGAARDEN, L. VAN & BIESHEUVEL, A. 1988 Voidage waves in mixtures of liquid and gas bubbles. In *Transient Phenomena in Multiphase Flow* (ed. N. Afgan), pp. 275–289. Hemisphere.

WIJNGAARDEN, L. VAN & KAPTEYN, C. 1990 Concentration waves in dilute bubble/liquid mixtures. *J. Fluid Mech.* **212**, 111–137.